United States Department of Agriculture

Equations for Predicting Internal Log Defect Measurements of Common Appalachian Hardwoods

Edward Thomas

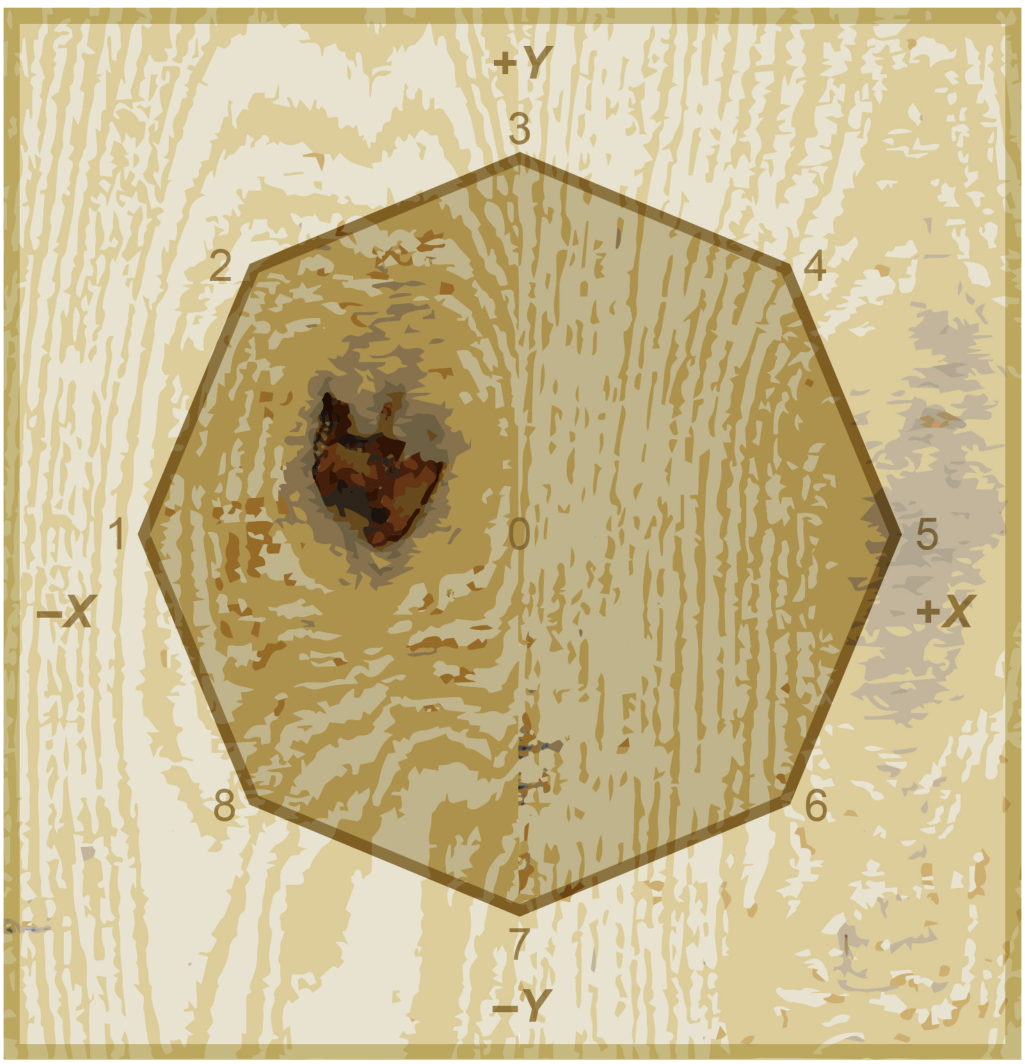

Forest Service | Forest Products Laboratory | Research Paper FPL–RP–687 | November 2016

Abstract

As a hardwood tree develops, surface defects such as wounds and branch stubs are overgrown or encapsulated into the tree. Evidence of such a defect remains present on the tree for decades, or for the life of the tree, in the form of bumps and changes in bark pattern. During this process, the appearance of the defect on the tree changes. The defect becomes flatter, the bark texture changes, and its dimensions change. This progressive change in appearance is predictable, permitting the size and location of the internal defect to be reliably estimated. Thus, the shape and size of the external defect indicator provide clues as to the type, shape, and size of the internal defect. Using log and defect data collected from six sites and four common Appalachian hardwood species—red oak, white oak, yellow-poplar, and sugar maple—a series of multiple linear regression models were developed to examine the internal–external defect relationship. The series of equations developed to predict attributes of the internal defect are presented.

Keywords: Appalachian, hardwood, log, defects

Contents

Conversion table

English unit	Conversion factor	SI unit
foot (ft)	0.3048	meter (m)
mile (m)	1.6093	kilometer (km)
square inch (in^2)	6.45	square centimeter (cm^2)

November 2016

Thomas, Edward. 2016. Equations for predicting internal log defect measurements of common Appalachian hardwoods. Research Paper FPL-RP-687. Madison, WI: U.S. Department of Agriculture, Forest Service, Forest Products Laboratory. 16 p.

A limited number of free copies of this publication are available to the public from the Forest Products Laboratory, One Gifford Pinchot Drive, Madison, WI 53726-2398. This publication is also available online at www.fpl.fs.fed.us. Laboratory publications are sent to hundreds of libraries in the United States and elsewhere.

The Forest Products Laboratory is maintained in cooperation with the University of Wisconsin.

Equations for Predicting Internal Log Defect Measurements of Common Appalachian Hardwoods

Edward Thomas, Research Scientist
Forest Products Laboratory, Madison, Wisconsin

Introduction

For many years, a major area of interest in hardwood research has been the development of methods to determine the defects contained within a log. Determining location, size, and severity of defects within a log would allow the value and recovery potential of the log to be determined before processing begins. Further, sawing of the log could then be optimized such that the maximum value is produced. In addition, accurate internal defect information would permit researchers to analyze, refine, and expand upon current log grading rules, multiproduct potential, stand differences, and impacts of silvicultural treatments on log and product quality in ways previously not possible.

One method of determining internal log defects is the use of x-ray computed tomography (CT) to examine the log (Araman et al. 1992). This process generates internal imagery where fine details are present that allow internal defect structures to be seen. The system also requires image processing and reconstruction systems to automate the detection of defects in the two-dimensional CT imagery "slices" and assemble a three-dimensional representation of the internal defects (Sarigul et al. 2005).

Researchers have studied the relationships among surface indicators and internal defect manifestation in depth for various hardwood and softwood species. Schultz (1961), in examining German beech (*Fagus sylvatica*), found that the ratio of bark distortion width to bark distortion length in this species is the same as the ratio of stem diameter when the branch was completely healed over to current stem diameter. However, for species with heavier irregular bark, such as hard maple, he found that it was difficult to judge the clear area above the defect in this manner.

Hyvärinen (1976) explored relationships among the internal features of grain orientation and height of clear wood above an encapsulated knot defect and the external features of surface rise, width, and length for sugar maple (*Acer saccharum*). Sugar maple defect data were collected from 44 trees obtained from three sites in upper Michigan. Hyvärinen used simple linear regression methods to find good correlations among clear wood above defects, bark distortion width, length, and rise measurements, as well as age, tree diameter, and stem taper. The best, simple correlation was with diameter inside bark (DIB) ($r = 0.66$) and a 0.66-in. standard error of estimate. Correlation was further improved by using a stepwise regression method. The final model ($r = 0.74$) used bark distortion vertical size and DIB as the most significant predictor variables for predicting encapsulation depth.

A similar study was conducted on a sample of 21 black spruce (*Picea mariana*) trees collected from a natural stand 75 km north of Quebec City (Lemieux et al. 2001). Three trees, each with three logs, were selected, from which a total of 249 knot defects were dissected and their data recorded. The researchers found better correlations between external indicator and internal characteristics in the middle and bottom logs than in the upper logs. Strong correlations ($r > 0.89$) were found among the length and width of internal defect zones and external features such as branch stub diameter and length. The defects were modeled as having three distinct zones corresponding to the manner in which the penetration angle changes over time in black spruce. The penetration angle is the angle at which a line through the center of the defect intersects the log surface.

Carpenter (1950) examined surface indicators and found that although the frequency and occurrence of surface indicators within a given species vary by region, in general the same indicator will be found with its defect in the underlying wood. Thus, although certain defect types may be more prevalent in some regions, the underlying manifestation of the defect would remain more or less consistent across regions. Further, growth rate varies from region to region (or site to site within the same region), so defect encapsulation rate will differ also. However, the rate at which the encapsulation occurs and the degree to which the defect is occluded or covered over by clear wood are indicated in the bark pattern. Shigo and Larson (1969) discovered that the ratio of defect height to width is a strong indicator of defect depth with respect to the radius of the stem at the defect (Fig. 1). The faster the diameter growth, the faster the defect is encapsulated and the faster the bark distortion pattern changes.

More recently, the relationships among external defect indicators and internal features were examined for the common Appalachian hardwood species of yellow-poplar (*Tulipifera liriodendron*) (Thomas 2008), red oak (*Quercus rubra*) (Thomas 2013), white oak (*Quercus alba*) (Thomas

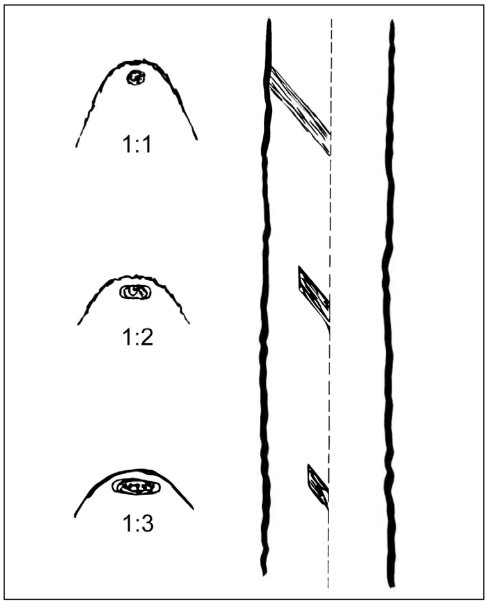

Figure 1. Encapsulation depth and stub scar relationship ratio (Shigo and Larson 1969).

2012), and sugar maple (*Acer saccharum*) (Thomas, in preparation). These studies consistently found statistically significant correlations between external indicators and internal features. The strongest correlations occurred with the most severe defect types (that is, overgrown knots, overgrown knot clusters, sound knots, and unsound knots). These defects are the most recent and therefore the least occluded. In almost all cases, correlations observed with severe defect types were significant ($\alpha < 0.01$). Conversely, the weakest correlations involved the least severe and most occluded defect types (that is, adventitious knots, adventitious knot clusters, light distortions, and medium distortions). In several cases, correlations between external and internal features failed to be statistically significant ($\alpha < 0.01$) for the less severe defect types. The prediction equations discovered by this research follow.

Methods

A total of 3,657 external defects were collected from six sites for the four species (Table 1). In some cases, samples for multiple species were collected from the same location. Red oak (*Quercus rubra*) defect samples were collected from two sites in West Virginia: West Virginia University Forest (WVU) near Morgantown (elevation 2,300 ft) and the Mead Westvaco Forest (MWF) near Rupert (elevation 3,200 ft). The two sites are separated by about 125 miles. Thirty-three trees were randomly selected from each site. Yellow-poplar defect samples were collected from two sites: the West Virginia University Forest (WVU) near Morgantown and the Camp Creek State Forest (CCSF) near Princeton (elevation 2,590 ft). The two sites are separated by approximately 220 miles. From each site, 33 trees were randomly selected. White oak (*Q. alba*) defect samples were collected from three sites in West Virginia: Fernow Experimental Forest located near Parsons, West Virginia, and two forests managed by Mead-Westvaco located in Fayette County, West Virginia, named F1 and F2. Thirty-two trees were randomly selected from the Fernow site, and 15 and 16 trees were randomly selected from the F1 and F2 sites, respectively. Sugar maple defect samples were collected from the Fernow and another forest managed by Mead-Westvaco located in Fayette County, West Virginia. Thirty-three trees were randomly selected from each of these sites.

Each tree was bucked into log lengths, and the logs were laser-scanned and manually diagrammed, recording the location and type of all defects. Numbers of defects by type were determined for the entire tree. Counts were used to develop a random sampling plan. The goal was to collect four defects of each type from each tree, whenever possible. For example, if there were eight sound knots on the tree, every second sound knot was selected. Of course, not all trees have four defects of every type. In other cases, selecting one defect would prevent another from being selected due to defect overlap. In these cases, preference went to the least common defect type on that tree, and a different occurrence of the second defect type was used. The numbers of defect samples obtained from each site by defect type is shown in Table 1. Once specific defects were selected from a tree, they were bucked from the tree and sliced into 1-in. boards (Fig. 2).

Sample Processing

All log surface defects were identified according to the characteristics defined by Carpenter et al. (1989). Once a log surface defect was located and classified, the section containing the defect was cut from the log. Typically, defect sections ranged from 12 to 24 in. in length. If, upon dissection, the inner portion of the defect was not completely contained within the section, the sample was discarded. For each sample, the following information was recorded: defect type, surface width (across grain), surface length (along grain), ring count and log diameter at defect location, and bark thickness. Next, a groove was cut into the top of the sample along the line from the center of the defect to the pith of the sample. The groove is used to measure the rake angle of the defect as it penetrates into the log sample and can be seen in Figure 2 at the top of the slices as a notch. The sample was then flat sawn into 1-in.-thick slices. This resulted in a photo series showing the defect penetrating the log (Fig. 2). The photo series shows a medium distortion defect. This sample had a slab thickness (distance from outer cambium to saw-kerf) of 0.9375 in. The faces of the first 2-in.-thick slices were clear of any defect and were not included in the photo series. For each slice, the depth (including any previous saw kerfs, slices, and bark slab), defect width, length, and distance of defect center to notch bottom were recorded. When a defect terminated between slices, it was assumed that it terminated at the halfway point through the slice.

Table 1. Number of defect samples examined by species, defect type, and location

Defect type	Red oak			Yellow-poplar			White oak				Sugar maple			Total all species
	WVU	MWV	Total	WVU	CCSF	Total	Fernow	F1[a]	F2[b]	Total	Fernow	MWV	Total	
Adventitious knot (AK)	54	51	105	66	75	141	41	11	23	75	14	48	62	383
Adventitious knot cluster (AKC)	27	47	74	68	59	127	82	21	75	178	46	51	97	476
Bump (BUMP)	1	6	7	1	3	4	30	11	14	55	40	33	73	139
Heavy distortion (HD)	52	46	98	60	74	134	31	6	12	49	25	22	47	328
Light distortion (LD)	2	37	39	6	98	104	41	7	26	74	49	57	106	323
Medium distortion (MD)	70	63	133	79	91	170	31	7	11	49	35	41	76	428
Overgrown knot (OK)	45	114	159	76	87	163	98	69	59	226	107	83	190	738
Overgrown knot cluster (OKC)	0	48	48	1	20	21	33	17	28	78	24	22	46	193
Sound knot (SK)	19	36	55	31	41	72	33	7	5	45	46	22	68	240
Sound knot cluster (SKC)	1	13	14	0	2	2	19	9	9	37	9	1	10	63
Unsound knot (UK)	30	31	61	33	6	39	23	0	8	31	12	21	33	164
Unsound knot cluster (UKC)	0	13	13	0	0	0	1	1	2	4	1	0	1	18
Wound (WOUND)	0	43	43	13	14	27	0	0	0	0	19	33	52	122
Total	301	548	849	434	570	1004	463	166	272	901	427	434	861	3615

[a]Fayette county, West Virginia, Site 1.
[b]Fayette county, West Virginia, Site 2.

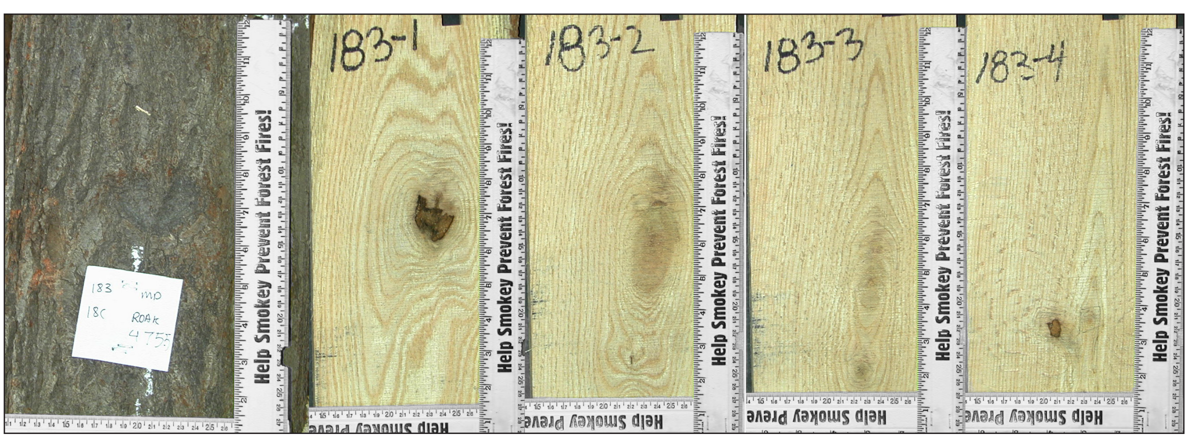

Figure 2. Surface indicator and internal defect slices for a medium distortion defect from a red oak log.

Modeling Statistics

A series of chi-squared tests were used to test for outliers in the internal/external data set (Komsta 2006). Any data points identified as a potential outliers were remeasured using the original sample for verification and corrected, if necessary. The data were grouped by defect type. Using the R statistical analysis program (R Development Core Team 2006), stepwise multiple linear regression analyses using the StepAIC function were used to test for correlations among surface indicators and internal features. StepAIC uses the Akaike Information Criterion (AIC) index to choose between competing models. As such, the index considers both the statistical goodness of fit and the number of parameters that have to be estimated to achieve the degree of fit by imposing a penalty for increasing the number of parameters. The independent variables used were surface indicator width (SWID), length (SLEN), rise (SRISE), and log diameter outside bark (DOB). These variables were selected because they are measurable during log surface inspection. Surface area (SWID * SLEN), volume (SWID * SLEN * SRISE), $SLEN^2$, $SRISE^2$, $SWID^2$, and all combinations of independent variables were examined as potential predictor variables. The dependent variables selected were penetration angle (RAKE), clear wood above defect (EDEPTH), total depth (TDEPTH), halfway point cross-section width (HWID), and halfway point cross-section length (HLEN). The halfway point is the geometric midpoint between the surface and total defect penetration depth. Using these variables, an internal model of a defect can be constructed and an approximate internal location determined (Fig. 3).

Within each defect type class, the data were randomly partitioned into two groups using the caTools package (Tuszynski 2006) for R. The first group contains approximately 66.7% of the sample and was used for model development and determining the internal−external feature correlation statistic (model development set). The second set contained the remaining records and was used for testing the prediction models (model validation set).

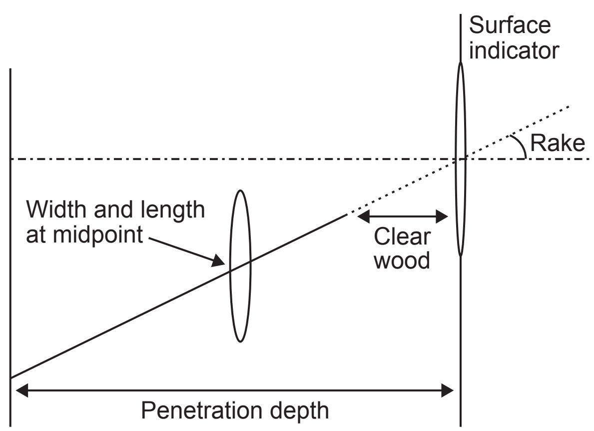

Figure 3. Illustration of internal features predicted by the model.

Discussion

Model development and testing correlation results are presented in Tables 2 and 3, respectively. A significance level of 1% was used for all tests. Correlation coefficient, significance, and mean absolute error (MAE) are reported for the model development and testing datasets. MAE is the mean of the absolute value of the residual errors for the fitted equation. As such, MAE indicates the ± error range that can be expected using the fitted equation to predict defect features. The significant independent variables for each species, defect, and internal feature are listed in Appendix I.

The fitted equations for predicting internal defect attributes of common defect types for the four species are presented in Appendix I. To use the equations, you must identify tree species, type of defect, diameter of the log adjacent to the defect, length, width, and rise of the defect. Carpenter et al. (1989) is a good reference on hardwood log defect identification and measurement. Hardwood log defects are typically measured using bark grain patterns for distortion-type defects and dimensions of the “bump” for knots and bumps (Fig. 4).

During data collection, the type (such as knot, hole, split) and condition (sound, decayed, or rotten) of the internal defect was noted for each internal defect slice (Fig. 2). Table 4 summarizes these data and lists the percentage of samples that were completely sound by species and defect type. With these data, one can roughly determine the likelihood that an internal defect will be completely sound. In our samples, yellow-poplar internal defects had the greatest chance of being completely sound, whereas sugar maple defects were the least likely to have a sound interior.

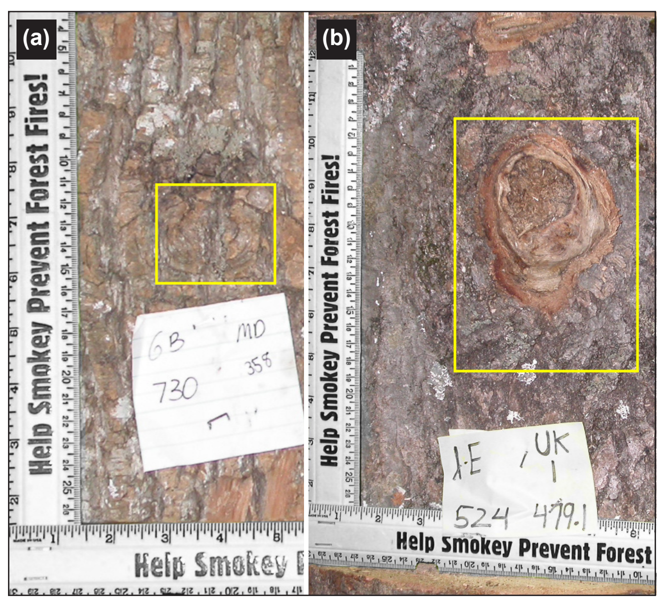

Figure 4. Measuring the surface indicators of (a) a bark distortion and (b) an unsound knot.

Table 2. Model development results for internal features by species and defect type

		Model development results[a]							
		Red oak		Yellow-Poplar		White oak		Sugar maple	
Defect type	Internal measurement	Multiple adjusted R^2	Mean absolute error	Multiple adjusted R^2	Mean absolute error	Multiple adjusted R^2	Mean absolute error	Multiple adjusted R^2	Mean absolute error
AK	Hwid	0.15	0.27	0.29	0.14	—	—	0.09	0.18
	Hlen	0.26	0.28	0.48	0.14	—	—	0.28	0.23
	Rake	0.12	5.04	0.20	4.09	—	—	***0.02***	6.21
	Depth	0.24	1.45	0.49	0.70	—	—	0.30	0.67
	Clear	***0.10***	1.27	***0.07***	0.78	—	—	0.16	1.06
AKC	Hwid	***0.11***	0.56	0.27	0.26	—	—	0.23	0.31
	Hlen	0.36	0.43	0.39	0.23	—	—	0.62	0.40
	Rake	0.20	7.15	—	—	—	—	***0.04***	10.39
	Depth	0.26	1.35	0.32	0.59	—	—	0.63	0.86
	Clear	0.06	1.12	0.15	0.64	—	—	***0.03***	0.80
BUMP	Hwid	—	—	—	—	0.31	0.43	0.16	0.70
	Hlen	—	—	—	—	0.31	0.98	0.20	2.10
	Rake	—	—	—	—	0.32	12.74	***0.03***	15.51
	Depth	—	—	—	—	0.81	0.57	0.28	1.18
	Clear	—	—	—	—	0.10	0.36	0.19	1.00
HD[b]	Hwid	0.55	0.20	0.36	0.21	0.31	0.33	0.10	0.25
	Hlen	0.47	0.43	0.34	0.34	0.30	0.64	0.15	0.37
	Rake	0.40	9.29	***0.08***	8.61	0.09	9.98	0.17	10.11
	Depth	0.27	0.86	0.76	0.44	0.67	0.68	0.66	0.45
	Clear	***0.08***	0.67	0.10	0.61	0.07	0.86	0.16	0.84
LD	Hwid	0.19	0.27	***0.03***	0.21	0.31	0.33	0.21	0.29
	Hlen	0.34	0.65	***0.02***	0.29	0.32	0.61	0.33	0.43
	Rake	***0.03***	10.06	***0.07***	8.12	0.17	10.43	***0.04***	13.11
	Depth	***0.09***	1.05	0.56	0.38	0.67	0.67	0.44	0.54
	Clear	***0.08***	0.94	0.18	0.81	0.18	0.95	***0.02***	0.96
MD[b]	Hwid	0.13	0.24	0.25	0.20	0.31	0.33	0.10	0.25
	Hlen	0.23	0.34	0.27	0.28	0.30	0.64	0.15	0.37
	Rake	0.10	10.50	—	—	0.09	9.98	0.17	10.11
	Depth	0.16	0.80	0.81	0.43	0.67	0.68	0.66	0.45
	Clear	0.10	0.86	0.25	0.73	0.07	0.86	0.16	0.84
OK	Hwid	0.53	0.29	0.55	0.24	0.57	0.41	0.40	0.32
	Hlen	0.40	0.67	0.49	0.40	0.41	0.96	0.34	0.74
	Rake	0.42	10.23	0.31	8.56	0.27	14.83	0.14	14.59
	Depth	0.45	0.96	0.76	0.41	0.44	0.83	0.56	0.54
	Clear	—	—	—	—	—	—	0.20	0.54
OKC[c,d]	Hwid	0.65	0.66	0.47	0.27	0.63	0.51	0.47	0.89
	Hlen	0.63	1.15	0.46	0.48	0.70	0.92	0.35	1.43
	Rake	***0.09***	9.70	0.22	11.13	0.45	11.78	0.18	15.30
	Depth	0.40	0.97	0.73	0.42	0.71	0.57	0.31	0.77
	Clear	—	—	—	—	—	—	0.37	0.39
SK[e]	Hwid	0.65	0.38	0.73	0.31	0.58	0.44	0.27	0.30
	Hlen	0.66	0.55	0.73	0.57	0.51	0.96	0.35	0.79
	Rake	0.45	9.18	0.70	8.75	0.43	12.16	0.13	11.11
	Depth	0.58	0.98	0.63	0.41	0.54	0.79	0.52	0.47
	Clear	—	—	—	—	—	—	—	—
UK	Hwid	0.74	0.30	0.70	0.28	—	—	—	—
	Hlen	0.87	0.74	0.65	0.66	—	—	—	—
	Rake	0.54	10.29	0.36	8.50	—	—	—	—
	Depth	0.63	0.72	0.70	0.48	—	—	—	—
	Clear	—	—	—	—	—	—	—	—

[a]Bold italic font indicates nonsignificant result at 99% significance level.
[b]HD and MD data pooled for white oak model.
[c]Red oak and hard maple models include overgrown, sound, and unsound knot clusters.
[d]OK and OKC data pooled for yellow-poplar model.
[e]OK and SK data pooled for white oak model.

Table 3. Model testing results for internal features by species and defect type

		Model testing results[a]							
		Red oak		Yellow-Poplar		White oak		Sugar maple	
Defect type	Internal measurement	Correlation coefficient R	Mean absolute error	Correlation coefficient R	Mean absolute error	Correlation coefficient R^2	Mean absolute error	Correlation coefficient R	Mean absolute error
AK	Hwid	0.52	0.26	0.53	1.89	—	—	***0.41***	0.20
	Hlen	***0.32***	0.41	0.44	0.25	—	—	***0.01***	0.27
	Rake	0.51	0.83	***0.11***	6.65	—	—	***0.03***	11.57
	Depth	***0.35***	1.57	0.74	1.05	—	—	0.58	1.03
	Clear	***0.40***	0.93	0.33	0.85	—	—	***0.05***	1.40
AKC	Hwid	0.61	0.82	0.29	0.12	—	—	***0.30***	0.39
	Hlen	***0.33***	0.81	0.56	0.26	—	—	***0.48***	0.38
	Rake	***0.12***	0.95	—	—	—	—	***0.11***	7.21
	Depth	0.80	0.90	0.74	1.06	—	—	0.75	0.60
	Clear	***0.37***	1.04	***0.18***	0.52	—	—	***0.10***	0.88
BUMP	Hwid	—	—	—	—	***0.36***	0.61	0.46	0.83
	Hlen	—	—	—	—	***0.33***	1.56	***0.29***	2.98
	Rake	—	—	—	—	***0.04***	16.39	***0.22***	16.06
	Depth	—	—	—	—	0.87	0.67	0.81	1.03
	Clear	—	—	—	—	***0.11***	0.74	***0.32***	1.15
HD[b]	Hwid	0.43	0.28	0.63	0.69	0.43	1.45	0.39	0.31
	Hlen	0.47	0.44	0.67	0.40	0.44	0.74	0.45	0.45
	Rake	0.68	8.54	***0.25***	5.85	***0.12***	11.53	***0.01***	14.40
	Depth	0.51	0.72	0.90	0.44	0.78	0.71	0.65	0.66
	Clear	***0.31***	0.62	0.38	0.23	***0.15***	0.87	***0.13***	0.97
LD	Hwid	***0.46***	0.41	0.59	0.36	***0.39***	0.44	0.64	0.28
	Hlen	***0.25***	1.09	0.60	0.19	***0.19***	0.98	0.78	0.44
	Rake	***0.14***	14.71	***0.26***	8.83	***0.21***	10.98	0.44	12.70
	Depth	***0.39***	1.18	0.77	0.46	0.82	0.70	0.70	0.69
	Clear	***0.01***	1.00	***0.37***	0.83	***0.29***	0.87	***0.05***	1.17
MD[b]	Hwid	0.56	0.29	0.35	0.31	0.43	1.45	0.39	0.31
	Hlen	0.61	1.78	0.37	0.28	0.44	0.74	0.45	0.45
	Rake	0.46	9.92	—	—	***0.12***	11.53	***0.01***	14.40
	Depth	0.63	0.75	0.84	0.44	0.78	0.71	0.65	0.66
	Clear	0.17	1.09	0.52	0.80	***0.15***	0.87	***0.13***	0.97
OK	Hwid	0.46	0.40	0.63	0.88	0.60	0.49	0.60	0.32
	Hlen	0.44	0.81	0.64	0.59	0.68	1.02	0.47	0.83
	Rake	0.60	11.82	0.46	8.84	0.48	12.66	0.36	14.39
	Depth	0.62	0.88	0.85	0.45	0.71	0.83	0.80	0.49
	Clear	0.17	0.04	—	—	—	—	0.38	0.54
OKC[c,d]	Hwid	0.58	0.81	0.44	0.89	0.79	0.53	0.80	0.87
	Hlen	0.49	1.35	0.47	0.60	0.87	0.83	0.71	1.62
	Rake	0.46	10.90	0.52	10.47	0.70	11.62	0.63	13.43
	Depth	***0.36***	1.14	0.86	0.45	0.75	0.73	0.78	0.47
	Clear	—	—	—	—	—	—	0.52	0.30
SK[e]	Hwid	***0.50***	0.75	0.87	0.66	0.71	0.50	0.77	0.33
	Hlen	0.61	0.71	0.79	0.82	0.70	1.07	0.79	0.91
	Rake	***0.07***	19.59	0.71	13.80	0.45	15.36	0.64	10.39
	Depth	***0.52***	1.45	0.78	0.56	0.68	0.95	0.80	0.53
	Clear	—	—	—	—	—	—	—	—
UK	Hwid	***0.08***	0.77	0.76	0.75	—	—	—	—
	Hlen	***0.37***	1.85	***0.45***	1.26	—	—	—	—
	Rake	0.55	12.22	***0.43***	9.71	—	—	—	—
	Depth	***0.45***	1.13	***0.45***	0.87	—	—	—	—
	Clear	—	—	—	—	—	—	—	—

[a]Bold italic font indicates nonsignificant result at 99% significance level.
[b]HD and MD data pooled for white oak model.
[c]Red oak and hard maple models include overgrown, sound, and unsound knot clusters.
[d]OK and OKC data pooled for yellow-poplar model.
[e]OK and SK data pooled for white oak model.

Table 4. External defects having internal manifestations that are completely sound, by species and defect type

	Number of defects where interior is completely sound (%)			
Defect type	Red oak	Yellow-poplar	White oak	Sugar maple
AK	58.1	91.1	73.3	61.7
AKC	62.2	82.5	66.3	58.6
BUMP	14.3	20.0	20.0	25.3
HD	43.4	43.5	38.8	25.0
LD	28.2	51.2	23.0	29.3
MD	35.6	46.9	34.7	23.8
OK	26.3	62.9	23.5	19.3
OKC	4.3	68.8	37.2	19.6
SK	51.8	88.0	72.3	46.6
SKC	15.4	N/A	75.7	9.1
UK	37.1	90.7	48.4	14.3
UKC	8.3	N/A	50.0	N/A
Wound	69.8	71.4	88.2	94.2
Overall	39.8	67.2	47.2	35.2

Summary

The severest defects with greatest impact on recovery are generally the most recent ones on a tree. Thus, severe log surface defect indicators provide the most clues about the nature of the encapsulated defect. Distortions and bumps are defects that have existed long enough to have become significantly encapsulated into the tree and their surface indicator obscured by growth. Thus, correlations are weaker among external indicators and internal features for less severe defects. This has been observed in all four species examined thus far.

The goal of this research was to develop models capable of predicting internal defect features using external defect measurements. These models were developed to complement automated scanning and detection research that locates severe defects on hardwood stems (Thomas and Thomas 2011). Two validation and confirmation studies have been conducted to examine accuracy of the internal defect predictions. The first compared predicted size and position of defects on digitally sawn board surfaces to size and position of defects on the actual sawn board surface (Thomas 2011a). The second examined the impact of different defect sizes and position, given the range of prediction errors, on the NHLA (NHLA 1998) grade and value of the board (Thomas 2011b).

In the first study, it was determined that the models can predict the occurrence of approximately 80% of all knot-type defects. Specifically, the models performed well at predicting the location of knots within a log, that is, the location of the defects on the resulting sawn board faces. The median error of the measured distance between the actual defect location and the predicted defect location was 0.875 in. Given the sizes of the knot defects, predicted and actual defect areas overlapped more often than not. The models' predictions for internal defect size were not as accurate but still acceptable in most instances. In 22 cases (32.8%), the error was less than 2.5 in^2. This error approximately corresponds to an error of 1.5 in. in defect length and width. The minimum size error observed was 0.02 in^2 and the maximum was 42.81 in^2. Overall, the median error for predicted defect area on the board faces was 5.59 in^2. This size of error is approximately 2.4 in. in defect width and length. In general, the model overestimates the size and therefore the severity of the internal defect.

The second study examined the impact of these potential errors on lumber value. Twenty-five additional red oak logs were scanned and digitally sawn. The sawing pattern for each log was used five times with different starting rotation angles: 0°, 22.5°, 45°, 90°, and 150°. For each log and sawing rotation, four defect prediction variations were examined:

1. Normal predicted values.
2. MAE for each feature added to the normal values. This resulted in a maximum size defect with a maximum location deviation.
3. MAE for each feature subtracted from the normal values. This resulted in a minimum size defect with a minimum location deviation.
4. Random amount of error ranging from −MAE to +MAE added to the normal values.

Depending on defect type, the mean absolute error of the prediction model varies from 0.4 to 1.8 in. in length and 0.3 to 0.8 in. in width at the defect cross-sectional size at the midpoint depth. For the random variations model, there were few instances of significant differences among all random defect variation size sets. In five instances, the differences were all between a single variation and all other variations. In only two instances was the minimum size variation in grade significantly different from all other size variations.

There were few significant differences among the random only sawn lumber sets. The random variations data are likely to be truer to reality than the nonrandom variations data that include the “best” and “worst” case scenarios. The greatest cross-sectional area error size for the prediction models is with knot clusters (Table 2). It could be expected that logs with more knot clusters might have greater variability in sawn lumber quality due to the larger range of variability permitted by the prediction models for these defect types.

Recent efforts at West Virginia University resulted in a computer program (Lin et al. 2011) that generates sawing solutions that optimize recovery according to National Hardwood Lumber Association (NHLA) lumber grades, which use the external defect scan and the predicted internal defect data from these models. As such, the prediction models allow the optimizer to know how deeply encapsulated a given defect is, how big it is, and how deep the defect penetrates the log. For example, the defect models allow the optimizer to know if a defect would be removed when a slab is sawn from the log.

References

Araman, P.A.; Schmoldt, D.L.; Cho, T.; Zhu, D.; Conners, R.W.; Kline, D.E. 1992. Machine vision systems for processing hardwood lumber and logs. AI Applications. 6(2): 13-26.

Carpenter, R.D. 1950. The identification and appraisal of log defects in southern hardwoods. Presentation delivered at the Deep South Section—Forest Products Research Society Annual Meeting, Memphis, TN. Oct. 26, 1950.

Carpenter, R.D.; Sonderman, D.L.; Rast, E.D. 1989. Defects in hardwood timber. Agric. Handb. 678. Washington, DC: U.S. Department of Agriculture. 88 p.

Hyvärinen, M.J. 1976. Measuring quality in standing trees—depth of knot-free wood and grain orientation under sugar maple bark distortions with underlying knots. Ann Arbor, MI: University of Michigan. 142 p. Ph.D. dissertation.

Komsta, L. 2006. Processing data for outliers. R News. 6(2): 10-13.

Lemieux, H; Beaudoin, M; Zhang, S.Y. 2001. Characterization and modeling of knots in black spruce (*Picea mariana*) logs. Wood and Fiber Science. 33(3): 465-475.

Lin, W.; Wang, J.; Thomas, R.E. 2011. A three-dimensional optimal sawing system for small sawmills in central Appalachia. In Fei, S., et al. eds. Proceedings, 17th central hardwood forest conference. Gen. Tech. Rep. NRS-P-78. Newtown Square, PA: U.S. Department of Agriculture, Forest Service, Northern Research Station: 67-76.

NHLA (National Hardwood Lumber Association). 1998. Rules for the measurement and inspection of hardwood and cypress lumber. Memphis, TN: National Hardwood Lumber Association.

R Development Core Team. 2006. R: a language and environment for statistical computing. Vienna, Austria: R Foundation for Statistical Computing. ISBN 3-900051-07-0. http://www.R-project.org. (March 1, 2012).

Sarigul, E.; Abbott, A.L.; Schmoldt, D.L.; Araman, P.A. 2005. An interactive machine-learning approach for defect detection in computed tomogaraphy (CT) images of hardwood logs. In: Proceedings of Scan Tech 2005 International Conference, Las Vegas, Nevada: 15-26.

Schultz, H. 1961. Die beureilung der Qualitätsentwicklung junger Bäum, Forstarchiv, XXXII (May 15, 1961). 97 p.

Shigo, A.L.; Larson, E.H. 1969. A photo guide to the patterns of discoloration and decay in living northern hardwood trees. Res. Pap. NE-127. Upper Darby, PA: U.S. Department of Agriculture, Forest Service, Northeastern Forest Experiment Station. 100 p.

Thomas, R.E. 2008. Predicting internal yellow-poplar log defect features using surface indicators. Wood and Fiber Science. 40(1): 14-22.

Thomas, R.E. 2011a. Validation of an internal hardwood log defect prediction model. In: Fei, S.; Lhotka, J.M.; Stringer, J.W.; Gottschalk, K.W.; Miller, G.W., eds. Proceedings, 17th central hardwood forest conference. Gen. Tech. Rep. NRS-P-78. Newtown Square, PA: U.S. Department of Agriculture, Forest Service, Northern Research Station: 77-82.

Thomas, R.E. 2011b. Testing and analysis of internal hardwood log defect prediction models. In: Proceedings of the 3rd international scientific conference on hardwood processing. Blacksburg, VA: Virginia Polytechnic Institute and State University: 85-94.

Thomas, R.E. 2012. Predicting internal white oak (*Quercus alba*) log defect features using surface defect indicator measurements. Forest Products Journal. 61(8): 656-663.

Thomas, R.E. 2013. Predicting internal red oak (*Quercus rubra*) log defect features using surface defect measurements. In: Miller, G.W.; Schuler, T.M.; Gottschalk, K.W.; Brooks, J.R.; Grushecky, S.T.; Spong, B.D.; Rentch, J.S., eds. Proceedings, 18th Central Hardwood Forest Conference. Gen. Tech. Rep. NRS-P-117. Newtown Square, PA: U.S. Department of Agriculture, Forest Service, Northern Research Station: 313-324.

Thomas, R.E. In preparation. Predicting internal hard maple (*Acer saccharum*) log defect features using surface defect indicator measurements. Forest Products Journal.

Thomas, L.; Thomas, R.E. 2011. A graphical automated detection system to locate hardwood log surface defects using high-resolution three-dimensional laser scan data. In: Fei, S.; Lhotka, J.M.; Stringer, J.W.; Gottschalk, K.W.; Miller, G.W., eds. Proceedings, 17th central hardwood forest conference. Gen. Tech. Rep. NRS-P-78. Newtown Square, PA: U.S. Department of Agriculture, Forest Service, Northern Research Station: 92-101.

Tuszynski, J. 2006. caTools: miscellaneous tools: I/O, moving window statistics, etc. R package version 1.14. http://cran.r-project.org/web/packages/caTools /caTools.pdf. (April 15, 2013).

Appendix I—Internal Defect Prediction Equations

Four surface defect measurements are used in the internal defect prediction equations presented in this section:

D Diameter of log at defect location

W Measured surface width of defect

L Measured surface length of defect

LW Measured surface length/measured surface width

R Measured surface rise of defect

All input and predicted measurements are in inches, with the exception of rake, which is in degrees.
The predicted measurement variables are as follows:

totalDepth The total penetration depth of the internal defect

rake The angle at which the defect penetrates the log; also known as penetration angle

clearDepth The depth of clear wood over the encapsulated internal defect; also known as encapsulation depth

midPtWidth The width of the internal defect at the penetration midpoint

midPtLength The length of the internal defect at the penetration midpoint

The equations for these variables are unique to each species and defect type. In addition, there are three internal variables that have equations that are common to all defects and species:

midPtDepth The middle point of the internal defect between clear depth and total depth

encapWidth Estimate of the internal defect structure width at the encapsulation endpoint

encapLength Estimate of the internal defect structure length at the encapsulation endpoint

They are calculated as follows:

$$\text{midPtDepth} = \text{totalDepth} - \frac{\text{totalDepth} - \text{clearDepth}}{2}$$

$$\text{endcapWidth} = \text{W} - \frac{\text{clearDepth}}{\text{midPtDepth}} * (\text{W} - \text{midPtWidth})$$

$$\text{endcapLength} = \text{L} - \frac{\text{clearDepth}}{\text{midPtDepth}} * (\text{L} - \text{midPtLength})$$

Appendix I.A—Yellow-Poplar Internal Prediction Equations

Adventitious knots

totalDepth = 0.429 + D*0.381 + R*W*5.322 − D*R*0.913

rake = 0.667 + R*29.330 + L*7.097 − R*W*20.609

clearDepth = −0.214 + D*0.098 − R*2.168

midPtWidth = 0.269 + W*L*0.114 − R*W*L*0.223

midPtLength = 0.394 − W*0.407 + W*L*0.269 + W*R*0.811 + W*D*0.014 − W*L*R*0.854

Adventitious knot clusters

totalDepth = 3.070 + D*0.099 − W*0.570 + D*W*0.071

rake = 2.3385 − W*1.620 + L*2.358 − W*L*0.589

clearDepth = 0.594 + W*0.404 − R*4.143 − L*0.155 − W*L*0.166 + R*L*1.526

midPtWidth = −1.137 + D*0.152 + W*0.162 − D*W*0.053

midPtLength = 0.356 + W*0.046 + W*L*0.041

Light distortions

totalDepth = 0.349 + D*0.392 + W*0.187

rake = 15.850 − W*5.479 + L*6.820

clearDepth = 8.244 − D*0.655 − W*3.489 + D*W*0.339

midPtWidth = 0.588 + L*0.075

midPtLength = 0.697 + L*0.094

Medium distortions

totalDepth = −0.788 + D*0.338 − L*0.158 + D*W*0.031

rake = 20.547 (Note: No rake correlation, uses mean value as substitute)

clearDepth = −3.513 + D*0.406 + W*0.947 − R*3.433 − D*W*0.072

midPtWidth = 0.129 + D*0.057 + L*0.066 − D*R*0.111

midPtLength = 0.071 + L*0.040 − L*W*0.100 + W*D*0.027 − D*R*0.176

Heavy distortions

totalDepth = 0.333 + D*0.444 − R*0.834

rake = 16.577 + D*0.710 + R*21.728

clearDepth = −0.080 + D*0.075 − R*1.401

midPtWidth = −0.757 + D*0.165 + L*0.309 − D*L*0.026

midPtLength = −0.868 + D*0.197 + L*1.237 + D*W*0.076 − D*L*0.112

Overgrown knots

totalDepth = −0.021 + D*0.415 + W*0.103

rake = 37.717 − D*1.701 + L*4.255

clearDepth = 0.164 − W*0.021 − L*0.030 + W* L*0.004

midPtWidth = −0.009 + L*0.200 − W*L*0.020 + W*D*0.012

midPtLength = 0.639 + L*D*0.025

Overgrown knot clusters

totalDepth = 0.203 + D*0.405 + W*0.089

rake = 8.312 + L*4.946 + R*23.769 − R*W*2.932

clearDepth = 0.0

midPtWidth = −0.313 + D*0.072 + L*0.173 + R*0.569 − L*R*0.188 + L*R*W*0.016

midPtLength = −0.420 + D*0.080 + L*0.298

Sound knots

totalDepth = 1.029 + D*0.331 + L*0.059

rake = −8.614 + W*5.235 + L*4.576 − W*L*0.347

clearDepth = 0.370 − W*0.056 − L*0.0519 + W*L*0.007

midPtWidth = 0.0279 − W*0.34760 + R*1.80206 + W*D*0.05631 − R*D*0.1857

midPtLength = −0.304 + D*W*0.045 − D*R*0.507

Sound and unsound knot clusters

Insufficient data to develop model for yellow-poplar.

Unsound knots

totalDepth = −0.821 + D*0.508 + L*0.207 − R*0.496

rake = 25.715 + L*3.458

clearDepth = 0.0

midPtWidth = −0.436 + L*0.329 + R*0.531 − R*W*0.068

midPtLength = −1.636 − W*0.104 + L*0.838 + R*0.730 − W*R*0.131

Appendix I.B—Red Oak Internal Prediction Equations

Adventitious knots

totalDepth = −1.375 + D*0.443 + W*0.984 − L*1.251 − R*2.389

rake = 0.9173 + L*5.390 + R*18.247 − R*W*8.148

clearDepth = −0.337 + D*0.169 − R*3.476

midPtWidth = 0.137 + L*0.380

midPtLength = −0.184 + W*0.214 + L*0.850 − W*L*0.317 + L*R*0.424

Adventitious knot clusters

totalDepth = 0.343 + D*0.351

rake = 7.505 + W*R*10.630 − R*D*1.955

clearDepth = 1.242 − R*2.171

midPtWidth = 0.374 + W*0.205 + R*0.825

midPtLength = 0.080 + L*0.496 + W*R*1.001 − L*R*1.359

Light distortions

totalDepth = 3.302 + D*0.233 − W*0.441 + R*7.710

rake = 21.649 − D*1.236 + D*W*0.295

clearDepth = 2.450 − L*0.501

midPtWidth = 0.033 + D*0.046 + L*0.192

midPtLength = −0.143 + L*0.873 − R*4.121

Medium distortions

totalDepth = 2.270 + D*0.158 + W*0.232

rake = 30.963 − D*1.940 + W*4.140

clearDepth = 1.493 + D*0.066 − W*0.481

midPtWidth = −0.121 + W*0.256 + L*0.342 − L*W*0.071

midPtLength = 0.730 + W*0.663 − D*0.145 + W*L*0.185 + D*L*0.056

Heavy distortions

totalDepth = 0.830 + D*0.236 + W*0.406

rake = 41.254 − D*3.588 + L*8.607

clearDepth = 2.405 − W*0.304 − L*0.968 + W*L*0.180

midPtWidth = 0.598 − D*0.039 − W*0.182 + L*0.183 + D*W*0.026

midPtLength = 0.607 + L*0.390 − D*0.070 + W*D*0.020

Bump uses overgrown knot equations.

Overgrown knots

totalDepth = 1.370 + D*0.172 − L*R*0.049 + D*W*0.025

rake = 20.210 − D*0.618 + L*3.838 + R*31.493 − D*R*2.415

clearDepth = 0.075 − W*0.011

midPtWidth = −0.252 + D*0.033 + L*0.231 + W*R*0.215 − L*R*0.221

midPtLength = −0.500 + L*0.550 − L*R*0.323 + W*R*0.292

Sound knots

totalDepth = 1.636 + L*1.340 − W*1.943 + W*D*0.233 − L*D*0.141

rake = 17.095 − D*2.622 + W*10.024 − W*L*0.438

clearDepth = 0.0

midPtWidth = 0.172 − W*L*0.008 + W*D*0.009

midPtLength = −0.489 + W*0.412 + R*0.778 − R*L*0.274 + W*R*L*0.020

Overgrown, sound, and unsound knot clusters

totalDepth = 3.158 + D*0.033 − L*W*0.020 + D*L*0.031
rake = 29.534 − D*1.386 + L*1.389
clearDepth = 0.0
midPtWidth = 2.008 + W*L*0.035 − D*L*0.016
midPtLength = −7.746 + D*0.926 + W*1.614 − L*0.812 + W*L*0.092 − W*D*0.129

Unsound knots

totalDepth = −7.441 + D*0.837 + L*0.754 + W*0.631 − W*L*0.038 − L*D*0.051
rake = 8.265 + W*10.349 − W*D*0.473
clearDepth = 0.0
midPtWidth = 0.036 + L*0.242 − W* L*0.030 − L*R*0.093 + L*D*0.023
midPtLength = 0.274 + W*0.182 + L*0.332 − R*W*0.227 + W*R*L*0.016

Appendix I.C—White Oak Internal Prediction Equations

Adventitious knots

totalDepth = 1.887 + D*0.236
rake = 0.433 + D*0.639 − W*4.258 + R*15.469
clearDepth = −0.273 + D*0.095 − R*1.514
midPtWidth = 0.240 + D*0.028
midPtLength = 0.544 + L*0.189

Adventitious knot clusters

totalDepth = 1.202 + D*0.359 − W*0.193
rake = 8.527 + L*1.389 − D*0.374
clearDepth = 0.222 − R*0.527 − L*0.074 + D*0.023
midPtWidth = 0.487 + W*0.220 − R*0.361
midPtLength = 0.943 + L*0.255 − R*0.399

Light distortions

totalDepth = .415 + D*0.423
rake = 19.756 − D*1.245 + W*7.516
clearDepth = −2.639 + D*0.187 + W*0.865 + L*0.621 − W*L*0.325
midPtWidth = 0.604 + W*0.375
midPtLength = 0.542 + W*0.762

Medium distortions

totalDepth = 0.830 + D*0.304 + L*0.355
rake = 32.458 − D*1.662 + L*4.575
clearDepth = −1.298 + D*0.148 + L*0.662 − D*W*0.049
midPtWidth = 0.533 + W*0.432 − W*D*0.023 + D*L*0.020
midPtLength = 1.409 + W*0.553 + W*L*0.160 − W*D*0.047

Heavy distortions

totalDepth = 0.724 + D*0.401
rake = 1.369 + L*17.145 − L*D*0.780
clearDepth = −1.100 + D*0.157 + W*L*0.275 − D*L*0.059
midPtWidth = 1.251 − R*1.722
midPtLength = 6.470 − W*2.386 − L*3.074 + R*49.641 + W*L*1.491 − W*R*30.131

Overgrown knots

totalDepth = 3.688 − W*L*0.028 − L*R*0.074 + L*D*0.049
rake = 17.399 + R*45.105 − R*D*2.437
clearDepth = 0
midPtWidth = −1.478 − D*0.066 + D*W*0.021
midPtLength = −4.201 − D*0.242 + D*L*0.033

Bump

totalDepth = 0.2175 + D*0.435 + W*L*0.008
rake = 25.601 − D*3.669 + W*7.076 + R*62.798 − W*R*7.077
clearDepth = 0.706 − R*0.758
midPtWidth = 1.128 + L*0.153
midPtLength = 2.608 − D*0.184 + L*0.747 − L*W*0.034

Sound knots

totalDepth = 1.636 + L*1.340 − W*1.943 + W*D*0.233 − L*D*0.141
rake = 17.095 − D*2.622 + W*10.024 − W*L*0.438
clearDepth = 0.0
midPtWidth = 0.172 − W*L*0.008 + W*D*0.009
midPtLength = −0.489 + W*0.412 + R*0.778 − R*L*0.274 + W*R*L*0.020

Overgrown, sound, and unsound knot clusters

totalDepth = 1.057 + D*0.340 + L*0.196480 − R*0.876 − L*W*0.021 + L*R*0.128
rake = 10.455 − D*1.045 + W*2.766 + R*7.477
clearDepth = 0.0
midPtWidth = 0.182 + W*0.362 + W*R*0.200 − W*D*0.033 − R*L*0.204 + D*L*0.031
midPtLength = −3.223 + D*0.231 + W*1.292 − D*W*0.099 + D*L*0.043

Overgrown and sound knots

totalDepth = 0.517 + D*0.338 + L*0.151
rake = 26.931 − D*1.566 + W*9.546 − R*28.627 − W*L*0.723 + R*L*4.230
clearDepth = 0.075 − W*0.013 − R*0.052 + W*R*0.008
midPtWidth = 0.061 + W*0.290 − R*0.661 + R*D*0.043
midPtLength = 0.585 + W*0.572 + L*0.286 − R*1.635 − W*L*0.044 + L*R*0.219

Unsound knots

totalDepth = −7.441 + D*0.837 + L*0.754 + W*0.631 − W*L*0.038 − L*D*0.051
rake = 8.265 + W*10.349 − W*D*0.473
clearDepth = 0.0
midPtWidth = 0.026 + L*0.242 − W*L*0.030 − L*R*0.093 + L*D*0.023 + L*W*R*0.008
midPtLength = 0.274 + W*0.182 + L*0.332 − R*W*0.227 + W*R*L*0.016

Appendix I.D—Sugar Maple Internal Prediction Equations

Adventitious knots

totalDepth = 1.02441 + D*0.34117
rake = 13.776 + D*0.53
clearDepth = 1.7892 − R*3.5782
midPtWidth = 0.31657 + W*0.09249
midPtLength = 0.72865 + L*0.33344 − D*0.04690

Adventitious knot clusters

$totalDepth = 3.677504 + D*0.014937 - L*0.407776$

$rake = 27.2754 - D*1.3517$

$clearDepth = 1.0130 - LW*0.5184$

$midPtWidth = 0.5462 + W*0.21048$

$midPtLength = 0.76418 + L^2*0.10306$

All distortion defects

$totalDepth = 2.823228 + D2*0.014982 + W*0.210660$

$rake = 20.258 + W*1.709 + R*118.573$

$clearDepth = 1.1806 - L*0.3373 + W*0.3080$

$midPtWidth = 0.24177 + D*0.02898 + L*0.17355$

$midPtLength = 0.95531 + L^2*0.06575$

Overgrown knots

$totalDepth = 0.596627 + D*0.392337 + W2*0.008252$

$rake = 21.4104 + L*2.7397$

$clearDepth = 0.01417 * D*0.10754 - W*0.15512$

$midPtWidth = -0.39180 + W*0.26011 - L*0.10510 + LW*0.92677$

$midPtLength = 0.81563 + L*0.25835$

Bump

$totalDepth = 2.9218 + D*0.22761$

$rake = 11.820 + W*2.622$

$clearDepth = -0.69581 + D*0.12328$

$midPtWidth = 2.175093 + L^2*0.011107 - R*1.683948$

$midPtLength = 4.01613 + L^2*0.05266 - R*5.70239$

Sound knots

$totalDepth = 0.25073 + D*0.39729 + L*0.09376$

$rake = 22.704 + W*2.723$

$midPtWidth = 0.7075 + W*0.1202$

$midPtLength = 0.11425 + W*0.35298$

Overgrown, sound, and unsound clusters

$totalDepth = -0.91407 + D*0.55747$

$rake = 14.0486 + L*1.9609$

$clearDepth = 1.1911 - LW*1.1718$

$midPtWidth = 0.072955 + D*W*0.025206$

$midPtLength = 1.210521 + W*L*0.037013$

Unsound knots

$totalDepth = 1.3800258 + D*0.3062578 + W*L*R*0.0021684$

$rake = 27.646 + W*2.483$

$midPtWidth = 0.8538 + W*0.1245$

$midPtLength = 0.9574 + W*0.3059$

Appendix II—Equations for Locating Defects Inside Logs

The following equations are used to determine the boundary points of an internal defect for a log. These equations assume that the log is centered on *X,Y* origin along the *Z* axis. In addition, the equations assume that the point *S*, the center point of a log surface defect, is known.

Then the following points can be determined:

I Interior center point

O_0 Center point of the outer defect circumference (Fig. 5)

$O_{1..8}$ Set of points describing the outer circumference of the interior log defect (Fig. 5)

M_0 Center point of middle describing circumference (Fig. 5)

$M_{1..8}$ Set of points describing the middle circumference of the interior log defect (Fig. 5)

$$d = \sqrt{S_x^2 + S_y^2}$$

$$\text{oOffset} = d * \tan(\text{rake})$$

$$\text{Origin}_x = 0.0$$

$$\text{Origin}_y = 0.0$$

$$\text{Origin}_z = S_z - \text{oOffset}$$

The Origin point is the projection of the log defect from the center of the surface point to the geometric center of the log, given the rake or penetration angle of the defect. The defect model developed here centers the defect structure about the *SO* line. Once *O* is known, the innermost point, *I*, and the middle cross-section center point, M_0, of the defect can be determined (Fig. 6).

$$z\text{Offset} = \text{totalDepth} * \tan(\text{rake})$$

$$r = \sqrt{\text{totalDepth}^2 + z\text{Offset}^2}$$

$$\Delta S\text{Origin} = \text{Origin} - S$$

$$\Delta SO = \sqrt{\Delta S\text{Origin}_x^2 + \Delta S\text{Origin}_y^2 + \Delta S\text{Origin}_z^2}$$

$$\text{Scale} = \frac{r}{\Delta SO}$$

$$I_x = S_x + \text{Scale} * \Delta S\text{Origin}_x$$

$$I_y = S_y + \text{Scale} * \Delta S\text{Origin}_y$$

$$I_z = S_z - z\text{Offset}$$

$$MZ\text{Offset} = \text{midPtDepth} * \tan(\text{rake})$$

$$p = \sqrt{MZ\text{Offset}^2 + \text{midPtDepth}^2}$$

$$\text{Scale} = \frac{p}{\Delta SO}$$

$$M_0 = S + \text{Scale} * \Delta S\text{Origin}$$

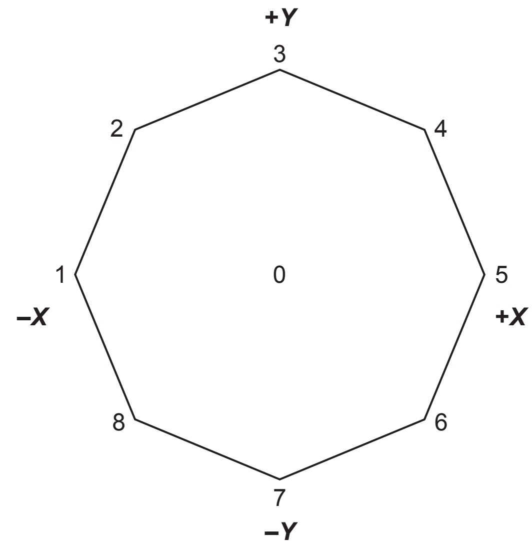

Figure 5. Arrangement of midpoint and outer point series that describes defect boundaries.

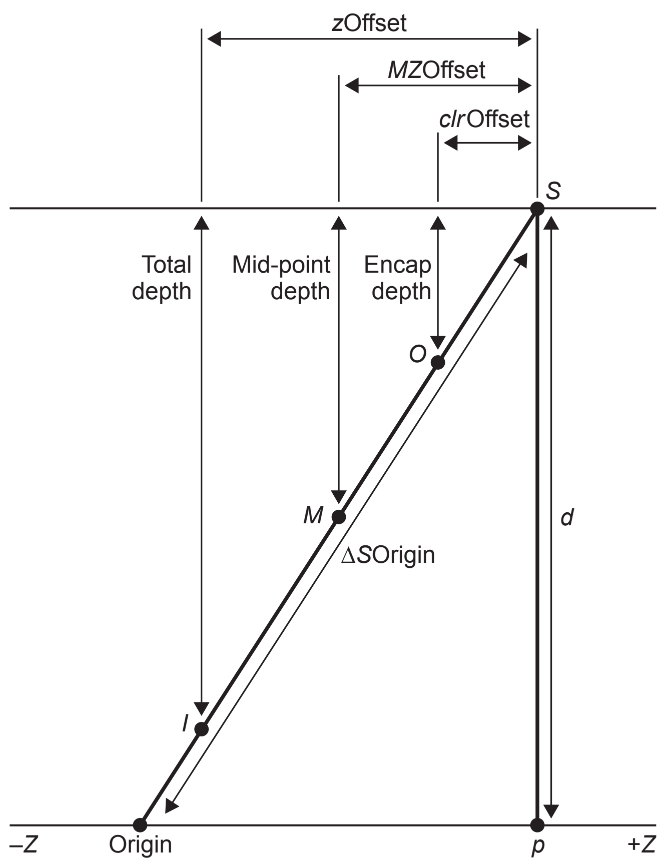

Figure 6. Graphical description of points and measurements used to position internal defects.

After the middle cross-section center point, M_0, of the defect is determined, the points, $M_{1..8}$, that describe the defect's middle boundary can be determined. Points M_1 and M_5 are found by first determining normal vectors N_1 and N_5 in the planes *ISP* and *IPS*, respectively (Fig. 5), where *P* is a point on the *Z* axis and *SP* is perpendicular to the *Z* axis:

$$P_x = 0.0$$
$$P_y = 0.0$$
$$P_z = S_z$$

$$N_1 = \nabla ISP$$
$$N_5 = \nabla IPS$$

$$M_1 = M_0 + N_1 * \text{midPtWidth}$$
$$M_5 = M_0 + N_5 * \text{midPtWidth}$$

Determine the points M_3 and M_7 using normal vectors for planes containing M_1, M_5, and *S*:

$$N_3 = \nabla M_1 M_5 S$$
$$N_7 = \nabla M_5 M_1 S$$

$$M_3 = M_0 + N_3 * \text{midPtLength}$$
$$M_7 = M_0 + N_7 * \text{midPtLength}$$

To solve for points M_2, M_4, M_6, and M_8, we find the distance of a diagonal point *T* from M_0, where the distance is the average of the midPtWidth and midPtLength:

$$\text{dDiag} = \frac{\text{midPtWidth} + \text{midPtLength}}{2}$$

$$D = M_1 - M_3$$
$$T = M_3 + D * 0.5$$
$$D = T - M_0$$

$$\text{Scale} = \frac{\text{dDiag}}{\sqrt{D_x^2 + D_y^2 + D_z^2}}$$

$$M_2 = M_0 + \text{Scale} * D$$

$$D = M_3 - M_5$$
$$T = M_5 + D * 0.5$$
$$D = T - M_0$$
$$M_4 = M_0 + \text{Scale} * D$$

$$D = M_5 - M_7$$
$$T = M_7 + D * 0.5$$
$$D = T - M_0$$
$$M_6 = M_0 + \text{Scale} * D$$

$$D = M_7 - M_1$$
$$T = M_1 + D * 0.5$$
$$D = T - M_0$$
$$M_8 = M_0 + \text{Scale} * D$$

If there is an encapsulation depth (that is, if clear wood has grown over the internal defect), then the next step is determining the outer center point of the defect:

$$\text{clrOffset} = \text{encapDepth} * \tan(\text{rake})$$

$$\text{Scale} = \frac{\sqrt{\text{encapDepth}^2 + \text{clrOffset}^2}}{\Delta SO}$$

$$O_0 = S + \text{Scale} * \Delta S\text{Origin}$$
$$\text{OuterWidth} = \text{encapWidth}/2.0$$
$$\text{OuterLength} = \text{encapLength}/2.0$$

If there is no encapsulation (that is, the defect extends to the surface of the log), then place the outer surface of the defect on the log surface:

$$O_0 = S$$
$$\text{OuterWidth} = \text{encapWidth}/2.0$$
$$\text{OuterLength} = \text{encapLength}/2.0$$

Solve for the O_1, O_3, O_5, and O_7 points using the N_1, N_3, N_5, and N_7 normal vectors calculated earlier when solving for the M_1, M_3, M_5, and M_7 points:

$$O_1 = O_0 + N_1 * \text{outerWidth}$$
$$O_5 = O_0 + N_5 * \text{outerWidth}$$

$$O_3 = O_0 + N_3 * \text{outerLength}$$
$$O_7 = O_0 + N_7 * \text{outerLength}$$

Last, solve for remaining outer defect boundary points:

$$\text{dDiag} = \frac{\text{outerWidth} + \text{outerLength}}{2}$$

$$D = O_1 - O_3$$
$$\text{Temp} = O_3 + D * 0.50$$
$$D = \text{Temp} - O_0$$

$$\text{Scale} = \frac{\text{dDiag}}{\sqrt{D_x^2 + D_y^2 + D_z^2}}$$

$$O_2 = O_0 + \text{Scale} * D$$

$$D = O_3 - O_5$$
$$\text{Temp} = O_5 + D * 0.50$$
$$D = \text{Temp} - O_0$$
$$O_4 = O_0 + \text{Scale} * D$$

$$D = O_3 - O_7$$
$$\text{Temp} = O_7 + D * 0.50$$
$$D = \text{Temp} - O_0$$
$$O_6 = O_0 + \text{Scale} * D$$

$$D = O_7 - O_1$$
$$\text{Temp} = O_1 + D * 0.50$$
$$D = \text{Temp} - O_0$$
$$O_8 = O_0 + \text{Scale} * D$$